JCTC Journal of Chemical Theory and Computation

Article

pubs.acs.org/JCTC

Method for Visualizing and Quantifying the Nonvalence Character of Excess Electrons

Thomas Sommerfeld*

Department of Chemistry and Physics, Southeastern Louisiana University, SLU 10878, Hammond, Louisiana 70402, United States

ABSTRACT: States formed by attachment of excess electrons to molecules or clusters can be broadly classified into valence and nonvalence states, but many of these states do have both, some valence and some nonvalence character. Here a new analysis scheme for this type of state is presented. It is based on considering the density of the excess electron as a function of the distance to the nearest atom, and this vantage point yields, in the first place, an intuitive picture akin to the well-known atomic radial distribution function, and, in the second place, a distance-from-the-atoms measure that is directly related to the nonvalence character of the excess electron. As a first test the analysis scheme is applied to the occupied orbitals of the water monomer, the water hexamer, and benzene, and its properties are contrasted to those of other frequently employed measures, such as the radius of gyration. Then its utility is demonstrated for three anions: $CH_3NO_2^-$, which has both a valence and a nonvalence state, $NaCl^-$, whose ground state has been classified as valence or nonvalence by different authors, and two conformations of the water hexamer anion, $(H_2O)_6^-$, the so-called AA isomer, which supports a surface state, and a Kevan-like structure, which has served as a model for a cavity state.

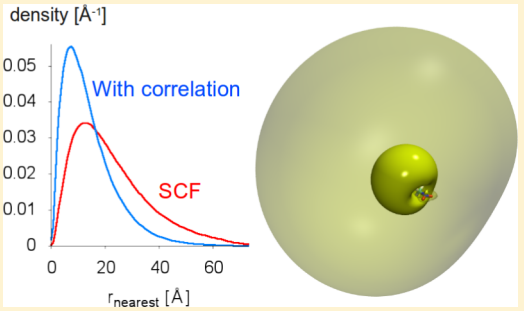

1. INTRODUCTION

Negative ions can be broadly classified into valence and nonvalence anions. In valence anions all electrons including the "excess" electron occupy valence orbitals, that is, orbitals with spatial extents similar to that of the molecular framework. Typical examples are OH^-, C_2^-, and NO_3^-. In contrast, in nonvalence anions the excess electron is bound by comparatively weak long-range forces, and occupies a diffuse, Rydberg-like orbital with an extent much larger than that of the molecule itself. Characteristic examples include dipole-bound anions such as CH_3CN^- or $(H_2O)_2^-$, quadrupole-bound anions such as the anti conformer of the succinonitrile anion, correlation-bound anions such as $(NaCl)_4^-$ or xenon cluster anions, and double Rydberg-bound anions such as $N_2H_7^-$.[1−6]

There are however many not so clear-cut cases. On the one hand, there are solvated electron-like systems such as electrons bound to larger water, ammonia, acetonitrile, or similar clusters, and for these species the spatial extent of the distribution of the excess electron can change smoothly from very diffuse to fairly compact depending on the dynamics of the structure of the solvent network (see, for example, refs 7−9). On the other hand, there are mixed cases, that is, states that have to some degree valence and to some degree nonvalence character. As a rule, the latter states can be understood as resulting from the coupling between two diabatic states, one pure valence state and one pure nonvalence state, and the mixing itself is typically controlled by a few selected nuclear degrees of freedom. One example is nitromethane, CH_3NO_2, where the ground electronic state of the anion changes from valence to nonvalence character depending on the wagging angle of the NO_2 group with corresponding dramatic changes in the electronic binding energy.[10,11] This interplay between the diabatic electronic states and the nuclear motion plays a major role in various electron-induced processes (see, for example, ref 12 and other articles in the topical issue of *Eur. Phys. J. D*).

For many of these anions an analysis scheme partitioning the density of the excess electron into valence and nonvalence contributions would be useful. Note that this partitioning is different from assigning the density of the excess electron to atoms, to basis function centers, or to certain basis functions. Schemes that have been used previously to analyze the excess electron of anions include (1) straightforward plotting of iso-contour maps or of iso-surfaces enclosing a fixed portion of the electron density, and judging valence character by eye; (2) calculation of expectation values such as $\langle r \rangle$ or the so-called radius of gyration, $r_{gy} = (\langle r^2 \rangle - \langle r \rangle^2)^{1/2}$, of the excess electron; (3) integrating the density enclosed within the atomic or van der Waals radii of certain atoms.

All of these schemes have their strengths and weaknesses. Iso-contour maps and iso-surfaces are well established work horses, but are obviously only able to convey qualitative impression, and even these can be misleading at times.[13] The radius of gyration is only indirectly related to the question of valence versus nonvalence character. It provides an averaged measure for the extent of the electron distribution, but to reach any conclusion about the nonvalence character this needs to be compared to the extent of the molecular framework. In particular if either the molecule or the electron distribution have an irregular shape, an averaged measure of the extent is

Received: September 4, 2013
Published: October 14, 2013

typically insufficient. Last, integrating the density close to an atom yields a valuable index regarding the valence character of that atom, but the result depends on an arbitrary cutoff, and it does not measure the spatial extent of the nonvalence portion of the density.

Here a new two-step analysis scheme is introduced, which rests on considering the density as a function of the distance to the nearest atom. In this way a distribution function is defined, which is analogous to the well-known radial density distribution of atoms, and which allows one to plot molecular density distributions as a function of a single variable. Computed formerly in a second step, the expectation value of this distribution, which is the same as the directly computed expectation value of the distance to the nearest atom, yields an index that measures valence character. By construction this index takes the shape of the molecule into account and does not involve any arbitrary cutoffs.

In the following the new analysis scheme will be applied to the distributions of valence and nonvalence electrons bound to several different molecules and molecular clusters. Ab initio methods used to compute these distributions and the geometries of the molecular systems are described in the next section. The analysis scheme itself is developed in section 3 and applied to the valence orbitals of the water monomer, the water hexamer, and the benzene molecule as initial tests cases in section 4. Excess electron distributions associated with three anions that have states with nonvalence character are analyzed in section 5, and section 6 concludes the discussion of this new analysis scheme.

2. AB INITIO METHODS AND GEOMETRIES

The new analysis scheme will be applied to the following molecules: H_2O, benzene, NaCl, CH_3NO_2, and two conformations of the water hexamer, $(H_2O)_6$. This section first describes these molecular systems and the particular geometries used, and then the ab initio methods employed to compute electron densities.

For H_2O, benzene, and NaCl the experimental gas phase geometries are used.[14] For CH_3NO_2 the geometries employed for neutral and anion are the minimum energy structures reported in ref 15 which have been obtained with the coupled-cluster with single, double (CCSD) and non-iterative triple excitations (CCSD(T)) method with Dunning's augmented correlation-consistent valence-polarized triple-ζ basis set. The two conformations of water hexamer anion considered are the so-called AA isomer, which is the isomer dominating the ion populations produced by many experimental sources,[16] and the so-called Kevan-model structure, which is a completely artificial, but nevertheless useful model system. The AA isomer is an open prism-like structure, where one water molecule accepts two hydrogen bonds, and thus has two hydrogen atoms, which it can point toward the excess electron. In the Kevan-like model structure used here, the oxygen atoms form a perfect octahedron, and each monomer points one OH bond directly toward the center (H-center distance is 2.1 Å) forming a "cavity". The other OH bond reduces the symmetry from perfectly octahedral, and the conformation used here has S_6 symmetry. (For more details see ref 17 where these two structures are referred to as as W6a and W6f.) Not only have these two structures served as test cases for newly developed methods for some time, but there are also intriguingly different electron correlation effects regarding their electron attachment energy,[17] a point that will be discussed in the light of the results of the new analysis scheme.

The one-electron densities discussed in the subsequent sections are either associated with self-consistent-field (SCF) orbitals from Hartree−Fock calculations or with natural orbitals from equation-of-motion coupled-cluster with single and double excitations calculations for electron attachment energies (EA-EOM-CCSD).[18] At the SCF level there are two different ways of describing excess electrons: the Koopmans's Theorem (KT) approximation, which uses the lowest unoccupied molecular orbital (LUMO) of the neutral, and unrestricted-spin Hartree−Fock (UHF) calculations, which produce a distinct singly occupied molecular orbital (SOMO) for the excess electron. UHF calculations were only performed for the nitromethane anion. Practically no spin-contamination was present for its dipole-bound state, but there was some spin-contamination for its valence state with an S^2 expectation value of 0.775. In the coupled-cluster calculations the core electrons were frozen in their closed-shell SCF orbitals. For all states considered here the EA-EOM-CCSD natural orbitals of the excess electrons could unambiguously be identified by their occupation numbers close to one, while "doubly occupied" and "unoccupied" natural orbitals had occupation numbers close to two and zero, respectively, where "close to" means ± 0.05 for all cases. The particular occupation numbers of the "singly occupied" natural orbitals studied here are 0.9992 for nitromethane, 0.9974 for $NaCl^-$, and 0.9931 and 0.9853 for the two $(H_2O)_6^-$ conformations considered.

The valence basis sets used in all calculations were Dunning's augmented correlation consistent double-ζ set (Aug-cc-pVDZ).[19] For the nonvalence states this set was further augmented with an extra system-dependent set of diffuse functions. For the dipole-bound state of CH_3NO_2 an 8s8p8d set of even-tempered functions (exponents between 0.1 and 1.554×10^{-5}; scaling factor of $(10)^{1/2}$) was placed 1 Å off the C atom along the CN bond. For NaCl, a 6s6p6d set with even tempered exponents (scaling factor $(10)^{1/2}$) was added to the Na Aug-cc-pVDZ basis starting for each angular momentum with the smallest exponents of the standard set. For the water hexamer an even tempered 5s4p set was used (even scaling factor of 5; first s and p exponents of 0.075 and 0.06, respectively). For the AA isomer this set was placed at the midpoint between the two H atoms of the double-acceptor (the "AA") water monomer. For the Kevan-like structure the extra diffuse set was placed at the symmetry center. Note that while the geometry of the water hexamer conformations is identical with that used in ref 17, the extra set of diffuse basis functions consists of different functions and is localized differently for the AA isomer. Version 1 of the CFOUR package was used for all electronic structure calculations.[20] Our own codes were used to process the "MOLDEN" output files from Cfour, and to perform the numerical integrations required to compute histograms and expectation values.

3. ANALYSIS SCHEME BASED ON THE DISTANCE TO THE NEAREST ATOM

Visualizing three-dimensional densities or distributions is a well-known challenge, be it speeds of gas molecules in the canonical ensemble or the electron density of the H 2s orbital to take just two examples most readers will be familiar with. Unlike more general cases, however, the high symmetry of these two familiar examples makes it easy to meet the visualization challenge. Just showing the distribution along

dx.doi.org/10.1021/ct400786n | J. Chem. Theory Comput. 2013, 9, 4866−4873

any line through the natural origin of the problem is already meaningful, even if these plots can still be deceptive, because one has to keep the integration weights and limits in mind. The most intuitive representation is probably the radial density or radial distribution function, because then, by definition, the area under the plotted curve directly represents probability.

In general, however, one does not have the luxury of high or even any symmetry, and regarding an orbital of an arbitrary molecule all that can be shown without further processing are either iso-contour maps of two-dimensional cuts through the density, or an iso-surface enclosing, say, 90% of the density. Both can convey a good qualitative sense of the shape and extent of the electron distribution, but both are of limited value when it comes to inferring the valence or nonvalence character of a distribution (c.f. ref 13).

To judge, by eye, the valence character of the density of an excess electron of an anion, $\rho(\vec{r})$, (or that of any other density) three requirements need to be fulfilled. First, a data reduction step is needed that allows one to plot ρ as a function of a single variable, say, ξ. Second, ξ must have a clear valence and a clear nonvalence range. An arbitrary cutoff between these regions, however, is not needed, on the contrary, it should be avoided as a feature of the scheme. If a cutoff is desired at a later stage, it can be imposed a posteriori. Last, $\rho(\xi)$ needs to be a distribution function, so that similar to the atomic case a ρ versus ξ plot is intuitive in the sense that area in the plot directly translates into probability.

One way to fulfill the three criteria for nonsymmetric molecules is to choose for ξ the distance to the nearest atom

$$r_{\text{nearest}}(\vec{r}) \equiv \min_{\alpha}(|\vec{r} - \vec{R}_{\alpha}|) \tag{1}$$

which is defined as the minimum of the distances to the nuclei of the molecule, where $\vec{R}_{\alpha}$ are the positions of the nuclei. One can now define the distribution $\rho(r_{\text{nearest}})$ analytically as a sum over Voroni cells, where in each cell the density is treated as a local radial density. It is however more instructive and of greater practical value to think of $\rho(r_{\text{nearest}})$ as a histogram that is computed from a list of tabulated density values. In fact, given this type of data, say a so-called cube file of the density, it is almost embarrassingly simple to compute a histogram approximation of $\rho(r_{\text{nearest}})$.

The input data required for the algorithm below are (1) an integration grid with N grid points, $\vec{r}_i$, which might be given explicitly or implicitly, (2) the density $\rho_i = \rho(\vec{r}_i)$ evaluated at the grid points, and (3) associated integration weights w_i such that

$$\sum_{i=1}^{N} \rho_i w_i \approx 1 \tag{2}$$

Algorithm:

(1) Choose a bin width δ, initialize all bins with 0.

(2) Loop over all grid points i.

(2.1) Obtain position $\vec{r}_i$, density ρ_i and weight w_i for grid point i.

(2.2) Calculate r_{nearest}.

(2.3) Add $\rho_i \times w_i$ to the bin with index closest to $r_{\text{nearest}}/\delta$.

Note that the largest distances possible are usually known beforehand, so that the number of bins needed can be estimated. For cube files dividing the space-diagonal of the cube (or box) by δ is more than on the safe side. Moreover, for cube files all weights are identical and equal to the cell volume, so that the algorithm becomes especially simple. However, while cube files are widely used in postprocessing and visualization, other grids such as those used to evaluate density functionals are certainly possible and these might be more convenient depending on the situation.

Having established a distribution function, $\rho(r_{\text{nearest}})$, with the desired properties, a further data reduction step can be taken by computing the average value of r_{nearest}, that is, the expectation value $\langle r_{\text{nearest}} \rangle$. This can either be done from the histogram, or with less numerical noise directly from the original tabulated density. The expectation value $\langle r_{\text{nearest}} \rangle$ provides a measure of how far an electron strays, on average, from the atoms, and clearly has the potential to serve as a valence index in comparisons of, say, excess electrons in different states or bound to different conformations.

4. VALENCE ORBITALS

Before applying the r_{nearest}-based analysis scheme to anions, the valence and core orbitals of the water monomer, the AA water hexamer, and the benzene molecule are examined. On the one hand, the properties of the analysis scheme are clarified, on the other hand, a baseline of what to expect for typical valence electrons is established.

Two density distribution functions, $\rho(r_{\text{nearest}})$ and $\rho(r)$, of all occupied SCF orbitals of the water molecule are compared in Figure 1. The first is the distribution function introduced in the last section, the second is the "atomic" radial density distribution computed with respect to the center of mass of

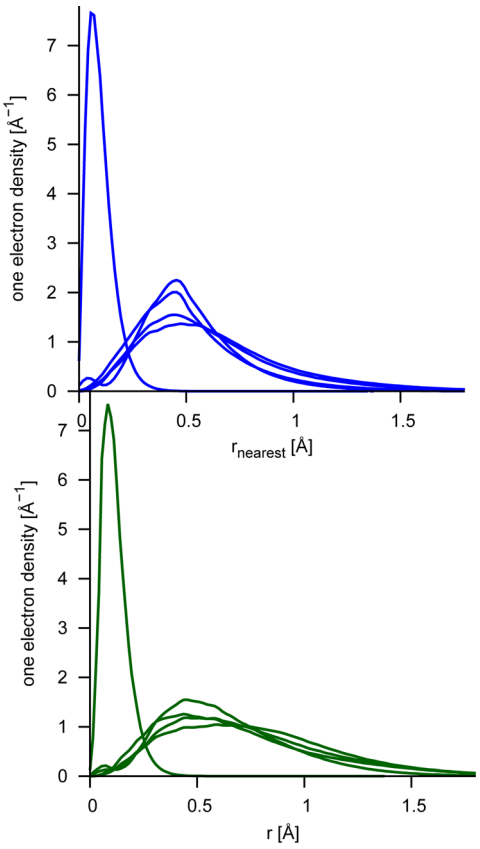

Figure 1. Density distribution functions of the occupied SCF orbitals of the water monomer. The upper panel shows the density as a function of the distance to the nearest atom, r_{nearest}, the lower panel shows the density as a function of the distance to the center of mass of the molecule.

dx.doi.org/10.1021/ct400786n | J. Chem. Theory Comput. 2013, 9, 4866−4873

the water molecule. The associated expectation values $\langle r_{nearest}\rangle$ and $\langle r\rangle$ are listed in Table 1 together with the associated radii of gyration. Since water is a fairly small molecule, the differences between the different measures cannot be striking, but even for water monomer $\rho(r_{nearest})$ shows clearly less pronounced tails than $\rho(r)$ (Figure 1), and the $\langle r_{nearest}\rangle$ expectation values are consequently consistently smaller than the corresponding $\langle r\rangle$ values.

Table 1. Expectations Values $\langle r_{nearest}\rangle$, $\langle r\rangle$, and the Radius of Gyration, r_{gy}, for the Five Occupied SCF Orbitals of the H_2O Monomer

	$\langle r\rangle$ [Å]	$\langle r_{nearest}\rangle$ [Å]	r_{gy} [Å]
$1a_1$	0.124	0.105	0.062
$2a_1$	0.648	0.536	0.302
$1b_2$	0.793	0.538	0.391
$3a_1$	0.759	0.630	0.399
$1b_1$	0.719	0.673	0.405

What is striking, though perhaps expected, are the differences when the same comparison is made for the water hexamer (Figure 2). One can think of the orbitals of the water hexamer in terms of linear combinations of localized monomer molecular orbitals (MOs), and therefore computing $\langle r\rangle$ or r_{gy} reflects rather the distance of the monomers, which contribute mostly to an MO, than how diffuse or compact an MO itself is. This can be clearly seen from the first six orbitals in Figure 2, which all correspond to different linear combination of oxygen 1s core orbitals, but nevertheless have $\langle r\rangle$ expectation values of up to 3.6 Å and radii of gyration of up to 5.8 Å. In other words, in this context $\langle r\rangle$ or r_{rg} do not provide a meaningful measure for the extent of the electron distributions, but rather for the extent of the molecule or cluster. In contrast, the $\langle r_{nearest}\rangle$ values in Figure 2 are for all orbitals very close to those of the monomer (Table 1), all six oxygen 1s core orbital combinations have $\langle r_{nearest}\rangle$ expectation values in the order of 0.1 Å, and results for all valence orbital fall into a 0.54−0.64 Å range. In addition, the valence orbitals also have distribution functions $\rho(r_{nearest})$, which are very similar to those of the monomer, in other words, the $r_{nearest}$-based data reduction reliably produces very similar distributions from very different MOs. There are some differences: the distributions found for the AA hexamer are slightly more compact than those found for the monomer, which can probably be attributed to the somewhat more polar nature of a water molecule in a hydrogen bonding network. Be that as it may, the $r_{nearest}$-based analysis of one-electron densities clearly establishes a valence signature, and the results in Figure 2 can serve as a baseline for comparison with the density of excess electrons attached to this and other water clusters.

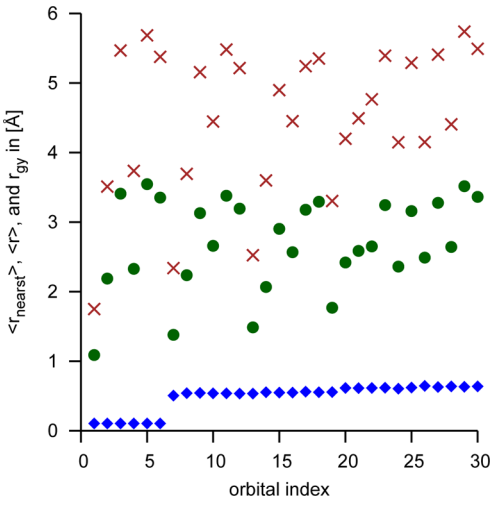

Figure 2. Expectations values $\langle r_{nearest}\rangle$ (blue diamonds) and $\langle r\rangle$ (green circles) as well as radii of gyration, r_{gy}, (brown crosses) for the 30 occupied orbitals of the AA-isomer of the water hexamer.

As a second case the benzene molecule is briefly considered. The $\langle r_{nearest}\rangle$ and $\langle r\rangle$ expectation values and the radii of gyration are shown in Figure 3. Even more clearly than the water hexamer results above, a look at the carbon 1s orbitals reveals that the $\langle r\rangle$ expectation value as well as the radius of gyration measure the radius of the benzene ring, whereas the $\langle r_{nearest}\rangle$ expectation value measures the extent of the carbon 1s orbital itself (0.14 Å). The same is true for the valence orbitals, but it is not quite as obvious. In addition, the $\langle r_{nearest}\rangle$ results for the valence orbitals clearly pick out the three π orbitals of benzene, which have $\langle r_{nearest}\rangle$ values 30−40% larger than those of σ orbitals. This is remarkable insofar as the lone-pair orbitals of water did not stand out in any particular way, and one would not expect the $\langle r_{nearest}\rangle$ expectation value to be particularly sensitive to the type of valence orbital in the first place.

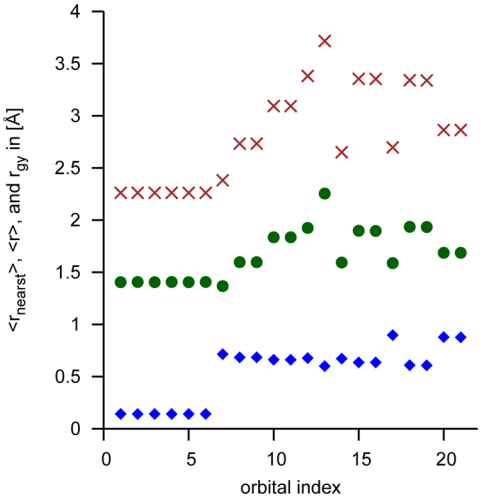

Figure 3. Expectations values $\langle r_{nearest}\rangle$ (blue diamonds) and $\langle r\rangle$ (green circles) as well as radii of gyration, r_{gy}, (brown crosses) for the 21 occupied orbitals of the benzene molecule.

To conclude this section, the results for the water hexamer and the benzene molecule demonstrate that the new analysis scheme works for one-electron densities derived from SCF orbitals. It provides a robust measure of compactness of MOs, and establishes a tentative 0.5−0.9 Å range one may expect for $\langle r_{nearest}\rangle$ expectation values of valence orbitals of first row nonmetal atoms.

5. RESULTS FOR THREE ANIONS

In this section the $r_{nearest}$-based analysis is applied to three anions that have either nonvalence states or states with nonvalence character: $CH_3NO_2^-$, $NaCl^-$, and the water hexamer anion, $(H_2O)_6^-$. These anions have been studied before and are well understood. Here, the primary goal is to see the $r_{nearest}$-based analysis method at work. The secondary goal is to

dx.doi.org/10.1021/ct400786n | J. Chem. Theory Comput. 2013, 9, 4866−4873

reinvestigate the three anions from a new vantage point, and to shed some new light on certain old controversies.

5.1. $CH_3NO_2^-$. Nitromethane is the prototypical anion that forms two states, a strongly bound valence state where the excess electron occupies a π^* orbital of the nitro group (vertical detachment energy of about 1 eV), and a dipole-bound with a much smaller electron binding energy (around 10 meV).[10,11,15,21] A natural basis for comparison is the highest occupied MO (HOMO) of neutral CH_3NO_2, which is a π orbital of the nitro group. The SOMO of the anion is also essentially a π^*-like orbital; however, the anion has a somewhat pyramidal NO_2 group. The $\rho(r_{nearest})$ distributions of the latter two orbitals are compared in the top panel of Figure 4, which

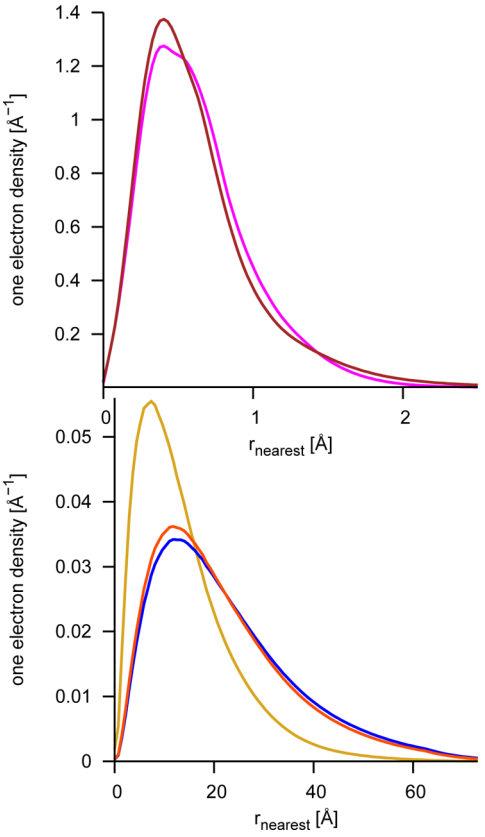

Figure 4. Density distribution functions $\rho(r_{nearest})$ for valence and dipole-bound orbitals of nitromethane. The upper panel compares the SCF HOMO of the neutral (purple) with the UHF SOMO of the anion (brown), where both species are at their respective equilibrium geometries. The lower panel compares the densities of a dipole-bound electron in the Koopmans's Theorem approximation (LUMO of the neutral (blue)) with the UHF SOMO associated with the dipole-bound state (red) and the natural orbital from an EA-EOM-CCSD calculation (golden). Note the different scales of the two plots.

shows that the SOMO of the anion seems as compact as the HOMO of neutral CH_3NO_2, and this finding is clearly reflected in the almost identical $\langle r_{nearest}\rangle$ expectation values of 0.69 Å and 0.68 Å for the two orbitals. In fact, similar to water and benzene, the $\langle r_{nearest}\rangle$ expectation values of all valence orbitals of the $CH_3NO_2^-$ anion including the SOMO fall into a narrow range of 0.57−0.70 Å, well within the tentative valence range established above. This behavior is insofar surprising in that it seems to contradict the well-known need for diffuse functions in calculations for anions as well as the much higher orbital energy of the SOMO in comparison with the energy of the other valence orbitals. The crucial distinction here is the nodal pattern, which influences the energy strongly, but has only a minor effect on expectation values such as $\langle r_{nearest}\rangle$. Loosely speaking, $\langle r_{nearest}\rangle$ is not distracted from the main character of an orbital by its oscillations, which makes $\langle r_{nearest}\rangle$ far more useful as an indicator of valence character than the orbital energy or a contour plot.

The dipole-bound state of $CH_3NO_2^-$ is known to be much more diffuse than the valence state, and it turns out that a completely different plotting range is needed to display $\rho(r_{nearest})$ (see lower panel of Figure 4). Using Koopmans's approximation the dipole-bound electron is represented by the LUMO of neutral CH_3NO_2. The associated density distribution function $\rho(r_{nearest})$ is shown in Figure 4, and with an $\langle r_{nearest}\rangle$ expectation value of 22.5 Å its density distribution is more than an order of magnitude more diffuse than that of the $CH_3NO_2^-$ valence state. Taking orbital relaxation effects into account in a UHF calculation reduces the $\langle r_{nearest}\rangle$ expectation value to 21.5 Å, but does not change the Koopmans picture significantly (Figure 4). Electron-correlation however can have a dramatic impact on nonvalence states,[2,4,22] but visualizing this effect or quantifying it beyond the electron binding energies has only rarely been attempted (see, for example, refs 4,23 for ab initio methods and ref 24 for model correlation). In most cases electron correlation increases the electron binding energy of nonvalence states, and CH_3NO_2 is a typical case (c.f. the general discussions in refs 2,4,22 and the specific calculations for CH_3NO_2 in section IV of ref 25). Figure 4 shows the associated change in the electron density distribution. In comparison with the SCF distributions, the EA-EOM-CCSD derived distribution is far more compact, which is expressed in three main differences. First, the maximum of the density distribution moves closer to the atoms; second, the height of this maximum is substantially increased; and third, the long-range tail of the SCF distribution is significantly reduced. This change is accompanied by a reduction of the $\langle r_{nearest}\rangle$ expectation value of the EA-EOM-CCSD natural orbital to 14.3 Å, much smaller than that of the SCF LUMO or UHF SOMO, yet still more than 1 order of magnitude larger than that of a typical valence state.

5.2. $NaCl^-$. Electrons bound to alkali halides were among the earliest examples of nonvalence states investigated,[26,27] and many of these polar diatomics support several negative ion states.[28] While there was no disagreement about the classification of the excited states of these anions as dipole-bound, there are open questions regarding the associated ground states, which have electron binding energies considered, by some, as too high for a dipole-bound state. Part of this discussion has been summarized in ref 4 and see also discussions on related systems in ref 28−30.

Here the density distribution function $\rho(r_{nearest})$ of the excess electron of $NaCl^-$ is, on the one hand, compared to the density distribution function of the HOMO of neutral NaCl, and, on the other hand, to the radial density distributions of the 3s and 3p orbitals of the Na atom (Figure 5). Specifically, the four orbitals compared in the figure are the SCF HOMO of NaCl, and natural orbitals from EA-EOM-CCSD calculations for the $NaCl^-$ anion and the Na atom. In contrast to CH_3NO_2, all distributions fit nicely on the same graph reflecting the much stronger binding in the $NaCl^-$ case. Note that the $\rho(r_{nearest})$ distribution function allows one to plot atomic and molecular densities in the same graph. Figure 5 shows that the HOMO of NaCl is clearly the most compact of the four considered, the Na

dx.doi.org/10.1021/ct400786n | J. Chem. Theory Comput. 2013, 9, 4866−4873

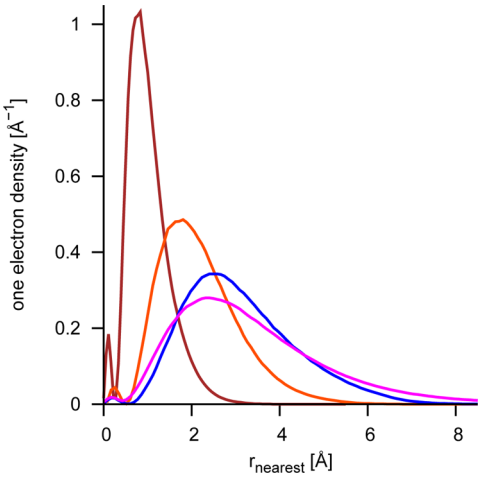

Figure 5. Density distribution functions $\rho(r_{nearest})$ associated with orbitals of NaCl and $NaCl^-$ and two atomic orbitals of the Na atom. Shown are, in the order of the heights of their maxima, the SCF HOMO of neutral NaCl (brown), the Na 3s orbital from a EA-EOM-CCSD calculation for the Na cation (red), the Na 3p orbital from the same calculation (blue), and the EA-EOM-CCSD natural orbital for the excess electron of $NaCl^-$ (purple).

3s orbital is next, and both the Na 3p orbital and the orbital of the excess electron of $NaCl^-$ are more diffuse than the former two with the Na 3p orbital having its maximum at the largest value of $r_{nearest}$, but the distribution of the $NaCl^-$ excess electron showing the most pronounced long-range tail.

The corresponding $\langle r_{nearest} \rangle$ expectation values of the four orbitals are 1.02, 2.22, 3.14, and 3.41 Å for the NaCl HOMO, Na 3s, Na 3p, and the $NaCl^-$ excess electron orbital, respectively, showing that the more pronounced tail dominates, and that the excess electron of $NaCl^-$ is roughly 10% more diffuse than the Na 3p orbital. Still in essence the conclusion about the anion's character depends on what one chooses as a basis of comparison. Comparison with the HOMO of neutral NaCl suggests characterization as a state with large nonvalence character and therefore classification as a dipole-bound state, possibly at the compact end of the dipole-bound spectrum. In contrast, comparison with the atomic orbitals of the sodium atom, in particular with the 3p orbital, suggests characterization as a somewhat diffuse valence state and therefore classification as an sp-hybrid orbital with very little dipole-bound character. (Of course there is yet another question, should the Na 3p orbital be counted as a valence orbital in the first place?)

What this discussion really shows is that a clean black-white classification of valence versus dipole-bound states, or in general other nonvalence states, is a moot point. Similar to the adiabatic change $CH_3NO_2^-$ undergoes during its wagging motion, the $NaCl^-$ ground state evolves from a valence state at large nuclear distances ($Na\cdots Cl^-$) to a dipole-bound state when the distance is short. At the equilibrium bond length this adiabatic change is so to speak in full swing, and the $NaCl^-$ ground state has mixed character. In this context, the $\langle r_{nearest} \rangle$ expectation value may not only turn out to be useful for comparing the spatial extent of different states quantitatively, but it may also provide a useful index to characterize the adiabatic change from a valence to a nonvalence state.

5.3. $(H_2O)_6^-$. Water cluster anions and their relation to the hydrated electron represent a huge research area, and different aspects have recently been reviewed.[9,31−34] Here the distribution of excess electrons bound to two conformations of the water hexamer are studied. One is a well-characterized dipole-bound or "surface" state, the AA isomer.[35] The AA isomer possesses one water monomer that accepts two hydrogen bonds, the AA monomer, and the excess electron is localized to a large extent off the AA monomer. The second conformation is the Kevan-structure, which is a small model system for an electron trapped in a locally octahedral solvent cavity, but which has no direct connection to experiment, because the solvating water monomers are fixed in space and are more importantly not members of a hydrogen bonding network. Benchmark ab initio vertical detachment energies (VDE) for these two structures are available in ref 17; the VDEs computed with the double-ζ set used here are listed in Table 2.

Table 2. Trends in the $\langle r_{nearest} \rangle$ Expectation Values and Associated Vertical Electron Detachment Energies (VDE) for Two Conformations of the Water Hexamer Anion[a]

	KT	EA-EOM-CCSD
	AA Isomer	
$\langle r_{nearest} \rangle$ [Å]	4.72	3.30
VDE [meV]	255	452
	Kevan Structure	
$\langle r_{nearest} \rangle$ [Å]	3.45	1.39
VDE [meV]	59	759

[a]The corresponding $\langle r_{nearest} \rangle$ expectation values for valence orbitals are in the 0.5−0.7 Å range (cf. Table 1 and Figure 2). The left column collects the Koopmans's Theorem results, the right column the results obtained with the EA-EOM-CCSD method.

First, the well-known vastly different electron correlation effects in the electron binding energies of the two conformations are also reflected in the $\langle r_{nearest} \rangle$ expectation values in Table 2. In the Koopmans picture the state supported by the Kevan-structure is only weakly bound, its $\langle r_{nearest} \rangle$ expectation value is 3.45 Å, and an accordingly large percentage of the excess electron density is not trapped within but rather localized outside the cavity. With electron correlation the binding energy is an order of magnitude higher, $\langle r_{nearest} \rangle$ is reduced by a factor of 2.5 to 1.39 Å, and much of the electron density is localized within the cavity, a complete change in the character of the excess electron distribution. Again, this change is reflected in $\langle r_{nearest} \rangle$ and can be visualized by plotting $\rho(r_{nearest})$. In contrast, for the AA isomer the changes for both, the electron binding energy and the $\langle r_{nearest} \rangle$ expectation value, are much less drastic.

In Figure 6 the density distribution functions $\rho(r_{nearest})$ associated with excess electrons bound to the two hexamer conformations are compared with a typical water valence orbital (in this case of the AA isomer). The distribution function associated with an excess electron attached to the AA isomer is clearly substantially more diffuse than that of a typical water valence orbital, the ratio between the corresponding $\langle r_{nearest} \rangle$ expectation values is larger than five (cf. Table 1 and Table 2), and the AA isomer can consequently be classified as dipole-bound. The Kevan-structure, on the other hand, falls between the two former states (Figure 6), and its $\langle r_{nearest} \rangle$ expectation value is only twice as large as that of a typical valence state. Thus, from a compactness point of view the excess electron of the Kevan structure is closer to a valence state than to a surface state even though its binding energy suggests the opposite (water valence electrons have binding energies in excess of 10 eV).

dx.doi.org/10.1021/ct400786n | J. Chem. Theory Comput. 2013, 9, 4866−4873

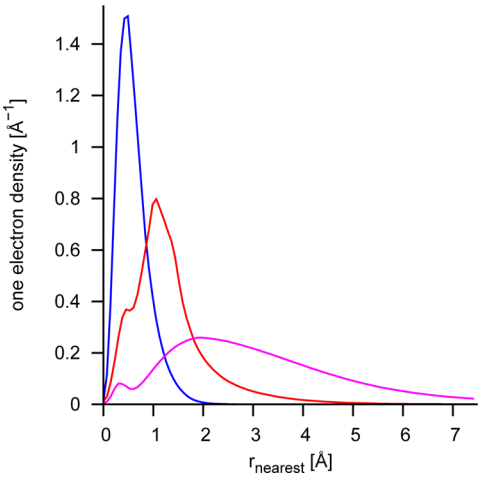

Figure 6. Density distribution functions $\rho(r_{nearest})$ associated with excess electrons bound to two conformations of the water hexamer. For the AA isomer the maximum of $\rho(r_{nearest})$ is close to 2 Å (purple line), for the Kevan-structure the maximum is roughly at 1 Å (red line). For both cases the excess electron density was obtained from the natural orbital of an EA-EOM-CCSD calculation. For comparison the density distribution of a typical water valence orbital (of the AA conformer) is shown (blue line). Note that $\rho(r_{nearest})$ will be very similar for all valence orbitals of the water monomer and both hexamer conformations (cf. section 4 and Figure 2).

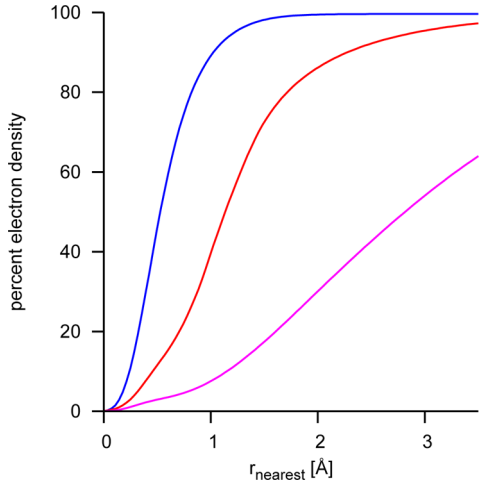

Figure 7. Integrated density distribution functions from Figure 6. For the AA isomer the increase is slowest (purple line), for the Kevan-structure it is faster (red line), and the fastest increase shown corresponds to a typical water valence orbital (in this case of the AA conformer; blue line).

Both excess electron distributions in Figure 6 show small peaks in the valence region. These peaks are related to so-called orthogonality spikes (or orthogonality tails) of the natural orbitals with respect to the valence orbitals. For typical nonvalence states the amount of density enclosed in these orthogonality spikes is in the order of a few percent or less, even if the electron binding energy is substantial (c.f.[13]), but if the distribution of the excess electron becomes more compact, say, in a nonvalence to valence transition situation, this percentage will become larger, and the excess electron will acquire a distinctly antibonding character. The percentage in the valence region can be estimated directly from the distribution graph (Figure 6), but can be seen even better if the integral

$$I(r_{nearest}) = \int_0^{r_{nearest}} \rho(r'_{nearest})\, dr'_{nearest} \qquad (3)$$

is plotted (Figure 7). Both figures show that the density of a valence orbital is mostly confined to distances of less than 1 Å from the atoms, that less than 10% of the excess electron of the AA state are in the valence region, and that the excess electron of the Kevan structure is somewhere in between. If a more concrete number is needed, a specific valence region must be defined in some arbitrary manner. One possibility is to define a cutoff from the 90% enclosing $r_{nearest}$ of a reference valence state, say the valence state displayed in Figure 7. With this definition the cutoff radius is 1.03 Å, the valence character of the excess electron of the AA isomer turns out to be 8%, and the valence character of the Kevan structure is found to be 40%. However, Figure 7 shows that these numbers should be taken with a grain of salt, as in particular the value for the Kevan structure depends strongly on the particular choice of the cutoff radius. Nevertheless, what is clear is that solvated electron states can acquire a substantial valence character through their orthogonality tails, and this behavior can be quantitatively seen in a graph of $\rho(r_{nearest})$ or of its integral.

In the context of solvated electron simulations it may be interesting to compare the ab initio distributions with results from one-electron model Hamiltonians (there are numerous; for recent work see, for example, refs 31,32,34,36). The reason is that in principle (really by virtue of the Phillips–Kleinman equation) these models should be able to describe correctly both, the energy of the excess electron and the associated density distribution outside the valence region, regardless of whether the excess electron has valence or nonvalence character. Inside the valence region the model wave function does not show the correct nodal pattern of the many-body orbital, but that of a node-less pseudo orbital, which nevertheless should integrate to the correct valence character. Practically however, most model potentials are written down in the spirit of a long-range dominated world, that is, with the vague idea that the excess electron does not have a substantial valence character, and more important, the fitting procedure of the model Hamiltonian is often biased toward examples with small valence character. While many model Hamiltonians have nevertheless performed well over a wide range of binding energies when compared to experimental data or ab initio results, some challenges regarding a balanced treatment of surface states versus cavity states have been noted,[24,31,36] and analyzing whether a model Hamiltonian reproduces not only the energy but also $\rho(r_{nearest})$ outside the valence region may be a way to further test and improve the models.

6. SUMMARY AND CONCLUSIONS

A new analysis scheme for the distributions of excess electrons geared toward distinguishing valence from nonvalence states has been introduced, but the new scheme can clearly be applied to any other density. It is based on considering the density of an excess electron as a function of the distance to the nearest atom, $r_{nearest}$, that is, it relies on a Voroni partitioning of the density. What is produced is, on the one hand, the distribution function $\rho(r_{nearest})$, and, on the other hand, the expectation value $\langle r_{nearest} \rangle$. Plotting the distribution function $\rho(r_{nearest})$ is an intuitive way of visualizing the valence or nonvalence character of an orbital completely analogous with the radial distribution function of atoms to which $\rho(r_{nearest})$ becomes equivalent in the

atomic limit. Here intuitive is meant as in contrast to contour plots, which can be counterintuitive, in particular if planes containing nuclei are shown, because the cusps and orthogonality tails associated with inner orbitals do typically look impressive in a contour plot, yet carry little weight in integrals over all space.

The expectation value $\langle r_{\text{nearest}} \rangle$ provides an index that measures the "distance" of an excess electron from a molecule. It is akin to the widely employed radius of gyration; however, $\langle r_{\text{nearest}} \rangle$ is more directly related to the question of the valence versus nonvalence character of a state because the radius of gyration becomes meaningful in this context only if it is compared to the size of the molecule, and even then there remain questions of relative orientation. With a grain of salt the radius of gyration measures the absolute size of the electron distribution, while $\langle r_{\text{nearest}} \rangle$ measures its size relative to the molecular system whatever the size and shape of the molecule may be.

The utility of the r_{nearest}-based analysis scheme is then demonstrated using the examples of $CH_3NO_2^-$, which has both a valence and a dipole-bound state, $NaCl^-$, whose ground state has some dipole-bound and some valence character, and two conformations of $(H_2O)_6^-$, one of which supports a surface-bound state, and one of which supports an interior or cavity state. In particular the visualization as a distribution function turns out to be a versatile tool that allows one to analyze electron correlation effects in nonvalence states, directly compare different states, different isomers, and even molecular with atomic density distributions, and judge valence character by-eye. If a more specific valence character than the compactness measure $\langle r_{\text{nearest}} \rangle$ is desired, say a valence character in percent, the integral of $\rho(r_{\text{nearest}})$ can be plotted, and after a somewhat arbitrary valence-nonvalence cutoff radius has been defined, the desired percentage can be directly read off the plot. Based on defining a cutoff from the 90% enclosing r_{nearest} of a typical water valence orbital, for the water hexamer anion a valence character of less than 10% is found for the surface state of the AA isomer, and of about 40% for the cavity state of the Kevan-model structure.

AUTHOR INFORMATION

Corresponding Author

*E-mail: Thomas.Sommerfeld@selu.edu.

Notes

The authors declare no competing financial interest.

ACKNOWLEDGMENTS

The author is grateful for stimulating discussions with Dr. William Parkinson. Acknowledgment is made to the donors of the American Chemical Society Petroleum Research Fund for support of this research.

REFERENCES

(1) Compton, R. N.; Hammer, N. I. Multipole-bound molecular anions. In *Advances in Gas-Phase Ion Chemistry*; Adams, N., Babcock, L., Eds.; Elsevier Science: New York, **2001**; pp 257−305

(2) Simons, J. *J. Phys. Chem. A* **2008**, *112*, 6401.

(3) Sommerfeld, T. *J. Chem. Phys.* **2004**, *121*, 4097.

(4) Sommerfeld, T.; Bhattarai, B.; Vysotskiy, V. P.; Cederbaum, L. S. *J. Chem. Phys.* **2010**, *133*, 114301.

(5) Bezchastnov, V.; Vysotskiy, V. P.; Cederbaum, L. S. *Phys. Rev. Lett.* **2011**, *117*, 133401.

(6) Ortiz, J. V. *J. Chem. Phys.* **2002**, *117*, 5748.

(7) Madarász, A.; Rossky, P. J.; Turi, L. *J. Chem. Phys.* **2009**, *130*, 124319.

(8) Marsalek, O.; Uhlig, F.; Jungwirth, P. *J. Phys. Chem. C* **2010**, *114*, 20489.

(9) Marsalek, O.; Uhlig, F.; VandeVondele, J.; Jungwirth, P. *Acc. Chem. Res.* **2012**, *45*, 23.

(10) Compton, R. N.; Carman, H. S., Jr.; Defrançois, C.; Abdoul-Carmine, H.; Schermann, J. P.; Hendricks, J. H.; Lyapustina, S. A.; Bowen, K. H. *J. Chem. Phys.* **1996**, *105*, 3472.

(11) Sommerfeld, T. *Phys. Chem. Chem. Phys.* **2002**, *4*, 2511.

(12) Sanche, L. *Eur. Phys. J. D* **2005**, *35*, 367.

(13) Sommerfeld, T.; Dreux, K. M. *J. Chem. Phys.* **2012**, *137*, 244302.

(14) *CRC Handbook of Chemsitry and Physics*, 92nd ed.; Haynes, W. M., Ed.; CRC Press, Taylor & Francis Group, Boca Raton, FL, 2011.

(15) Adams, C. L.; Schneider, H.; Ervin, K. M.; Weber, J. M. *J. Chem. Phys.* **209**, *130*, 074307.

(16) Hammer, N. I.; Shin, J.-W.; Headrick, J. M.; Diken, E. G.; Roscioli, J. R.; Weddle, G. H.; Johnson, M. A. *Science* **2004**, *306*, 675.

(17) Vysotskiy, V. P.; Cederbaum, L. S.; Sommerfeld, T.; Voora, V. K.; Jordan, K. D. *J. Chem. Theory Comput.* **2012**, *8*, 893.

(18) Nooijen, M.; Bartlett, R. J. *J. Chem. Phys.* **1995**, *102*, 3629.

(19) Dunning, T. H., Jr. *J. Chem. Phys.* **1989**, *90*, 1007.

(20) CFOUR, a quantum chemical program package written by Stanton, J. F.; Gauss, J.; Harding, M. E.; Szalay, P. G.; with contributions from Auer, A. A.; Bartlett, R. J.; Benedikt, U.; Berger, C.; Bernholdt, D. E.; Bomble, Y. J.; Christiansen, O.; Heckert, M.; Heun, O.; Huber, C.; Jagau, T.-C.; Jonsson, D.; Jusélius, J.; Klein, K.; Lauderdale, W. J.; Matthews, D. A.; Metzroth, T.; O'Neill, D. P.; Price, D. R.; Prochnow, E.; Ruud, K.; Schiffmann, F.; Stopkowicz, S.; Tajti, A.; J. Vázquez; Wang, F.; Watts, J. D. and the integral packages MOLECULE (Almlöf, J.; Taylor, P. R.), PROPS (Taylor, P. R.;), ABACUS (Helgaker, T.; Jensen, H.J. Aa., Jørgensen, P.; Olsen, J.), and ECP routines by Mitin, A. V.; C. van Wüllen. For the current version see http://www.cfour.de.

(21) Adamowicz, L. *J. Chem. Phys.* **1989**, *91*, 7787.

(22) Gutowski, M.; Skurski, P.; Boldyrev, A. I.; Simons, J.; Jordan, K. D. *Phys. Rev. A* **1996**, *54*, 1906.

(23) Sommerfeld, T. *J. Phys. Chem. A* **2008**, *112*, 11817.

(24) Sommerfeld, T.; DeFusco, A.; Jordan, K. D. *J. Phys. Chem. A* **2008**, *112*, 11021.

(25) Stokes, S. T.; Bowen, K. H.; Sommerfeld, T.; Ard, S.; Mirsaleh-Kohan, N.; Steill, J. D.; Compton, R. N. *J. Chem. Phys.* **2008**, *129*, 064308.

(26) Jordan, K. D.; Wendoloski, J. *Mol. Phys.* **1978**, *35*, 223.

(27) Jordan, K. D.; Seeger, R. *Chem. Phys. Lett.* **1978**, *54*, 320.

(28) Gutsev, G. L.; Nooijen, M.; Bartlett, R. J. *Chem. Phys. Lett.* **1997**, *276*, 13.

(29) Jordan, K. D.; Wang, F. *Annu. Rev. Phys. Chem.* **2003**, *54*, 367.

(30) Desfrançois, C.; Bouteiller, Y.; Schermann, J. P.; Radisic, D.; Stokes, S. T.; Bown, K. H.; Hammer, N. I.; Compton, R. N. *Phys. Rev. Lett.* **2004**, *92*, 083003−1.

(31) Herbert, J. M.; Jacobson, L. D. *Int. Rev. Phys. Chem.* **2011**, *30*, 1.

(32) Turi, L.; Rossky, P. J. *Chem. Rev.* **2012**, *112*, 5641.

(33) Young, R. M.; Neumark, D. M. *Chem. Rev.* **2012**, *112*, 5553.

(34) Abel, B.; Buck, U.; Sobolewski, A. L.; Domcke, W. *Phys. Chem. Chem. Phys.* **2012**, *14*, 22.

(35) Hammer, N. I.; Roscioli, J. R.; Johnson, M. A. *J. Phys. Chem. A* **2005**, *109*, 7896.

(36) Voora, V. K.; Cederbaum, L. S.; Jordan, K. D. *J. Phys. Chem. Lett.* **2013**, *4*, 849.